DETERMINATION OF STRESS INTENSITY FACTORS FOR CRACKS EMANATING FROM HOLES IN FINITE THICKNESS PLATES

by

Shau-Fen Gou

Thesis submitted to the Graduate Faculty of the Virginia Polytechnic Institute and State University in partial fulfillment of the requirement for the degree of

MASTER OF SCIENCE

in

Engineering Mechanics

APPROVED:

C. W. Smith, Chairman

E. G. Henneke

K. L. Frair

December 1977

Blacksburg, Virginia

ACKNOWLEDGEMENT

The author wishes to express his sincere appreciation to his advisor, Professor C. W. Smith, for his valuable guidance and discussion for this work. Thanks go also to Dr. E. G. Henneke and Dr. K. L. Frair and are due to Professor W. H. Peters for his advice and technical assistance in the preparation of experiments. In addition the support of National Aeronautics and Space Adminstration at Langley and that of National Science Foundation, under the Grant No. NSG 1024 and ENG. 76-20824, respectively, were essential to the completion of this study.

CONTENTS

LIST OF TABLES

LIST OF FIGURES

NOMENCLATURE

n,p,z		Local rectangular cartesian coordinates along the flaw border
σ_{ij}	$i,j=n,z.$	Stress components in plane normal to flaw surface and flaw border near crack tip (kPa)
σ^{o}_{ij}	$i,j=n,z.$	Part of regular stress field near crack tip (kPa)
r,θ		Polar coordinates measured from crack tip
τ_{max}		Maximum shear stress in plane normal to flaw surface and flaw border near crack tip (kPa)
$\bar{\sigma}$		Remote normal stress (kPa)
K_{ap}		Apparent Stress Intensity Factor ($kPa\text{-}mm^{1/2}$)
K_I		Mode I Stress Intensity Factor ($kPa\text{-}mm^{1/2}$)
N		Stress fringe order
f		Material fringe constant (g/mm/order)
T		Slice thickness (mm)
α		Angle of rotation from point of flaw intersection with plate (degrees)
c		Crack length along the plate (mm)
a		Crack depth in the hole (mm)
$\bar{r}$		Radius of hole (mm)
t		Plate thickness (mm)

INTRODUCTION

Cracks emanating from the intersection between a cylindrical hole and a free surface of finite thickness plates are considered to be one of the most prevalent problems in the aerospace industry. According to a survey (2), more than 30% of aerospace failures resulted from this problem. Although there are no closed from solutions available in the literature, photoelasticity lends itself naturally as an appropriate method for the solution of this problem. The earliest study of the stress field at crack tips by photoelasticity was done by Post (3) and Wells and Post (4). The use of photoelasticity to extract the stress intensity factor (SIF) from photoelastic data was first suggested by Irwin. Later Fessler and Mansell (5), Marloff, et al (6) and Kobayashi and his associates (7)-(10) extended this work. Then over a period of years, Smith and his associates (11)-(18) developed the Taylor Series Correction Method (TSCM) to deal with three dimensional problems. The present author used the stress freezing photoelastic technique coupled with a computer program to extract the SIF from the corner crack at the edge of the hole. It is well known that the SIF, the parameter which dominates the stress distribution around the crack tip, plays a very important role in fracture mechanics. Once the SIF's are known for specific geometries in this problem, two types of analysis could be done (19):

1) Determine the critical crack size which would cause catastrophic failure.
2) Predict the approximate life of the cracked component before the crack grows to critical size.

The general procedure for dealing with the three dimensional problems in many of the numerical and empirical techniques is to introduce some correction factors to modify a known two dimensional solution of a simpler problem. Others will impose many assumptions to limit the complexity of the problem. Some of these numerical approaches will be described briefly in the appendix of this paper. A comparison of prior results (Table II) shows that the greatest discrepancies in the several solutions occur when the crack shape approaches a quarter circle. The purpose, then, of this paper is to examine this geometry in detail.

ANALYTICAL BACKGROUND

It was shown in Irwin's paper (20) that the elastic stress field for small strain around the crack tip was dominated by the SIF. The stress equations in Mode I can be expressed by

$$\sigma_{nn} = \frac{K_I}{(2\pi r)^{1/2}} \cos\frac{\theta}{2}\left(1 - \sin\frac{\theta}{2}\sin\frac{3\theta}{2}\right) - \sigma^o_{nn}$$

$$\sigma_{zz} = \frac{K_I}{(2\pi r)^{1/2}} \cos\frac{\theta}{2}\left(1 + \sin\frac{\theta}{2}\sin\frac{3\theta}{2}\right) - \sigma^o_{zz} \qquad (1)$$

$$\sigma_{nz} = \frac{K_I}{(2\pi r)^{1/2}} \sin\frac{\theta}{2}\cos\frac{\theta}{2}\cos\frac{3\theta}{2} - \sigma^o_{nz}$$

The notations are shown in Fig. 1 (21). Moreover, the value of σ^o_{nn}, σ^o_{zz}, σ^o_{nz} represent the contribution of the regular part of the stress field to the components of stress near the crack tip and will be different from point to point along the crack front. In general σ^o_{ij} may be expressed in the form of a Taylor Series Expansion $\sum_{n=o}^{m} B_n r^{n/2}$, but, to date, only the leading term B_o has been found necessary. From equations (1), we may compute the maximum shear stress in n-z plane by using equation (2)

$$\tau_{max} = \frac{1}{2}\left((\sigma_{nn} - \sigma_{zz})^2 + 4\,\sigma_{nz}^2\right)^{1/2} \qquad (2)$$

When the polarized light passes through the model under load, a fringe pattern which represents the constant maximum shear stress along the same

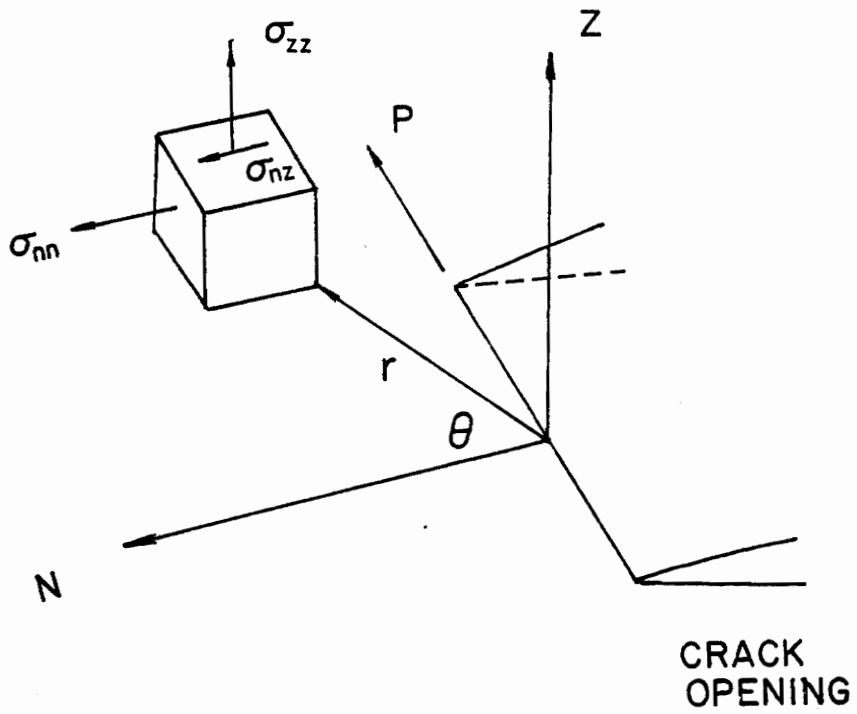

Fig. 1 Notation for Local Stress Field near Crack Tip

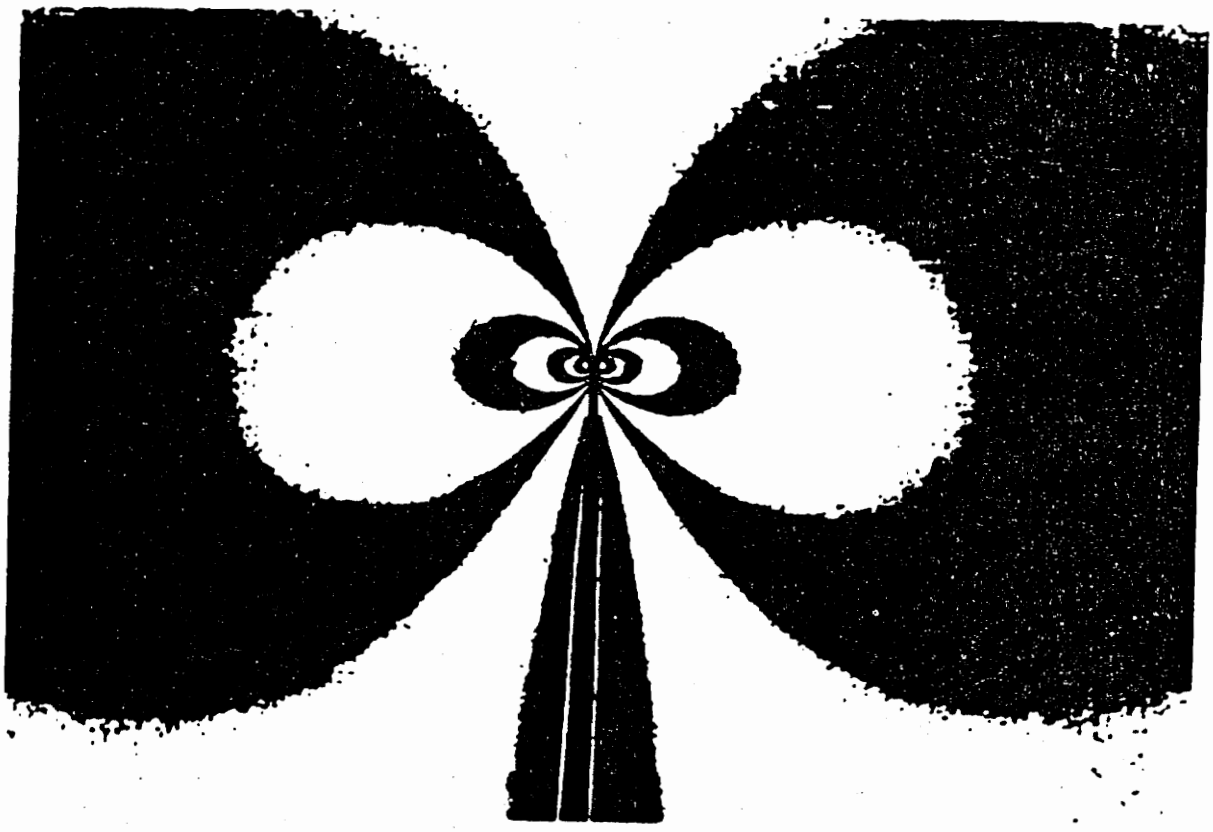

Fig. 2 Mode I Fringe Spreading Normal to Crack

dark loop will be seen in the model. By observing the typical Mode I fringe loops in (Fig. 2), the fringes are seen to spread the most along the line $\theta = \frac{\pi}{2}$. After substituting equations (1) into equation (2), evaluating at $\theta = \frac{\pi}{2}$, expanding in series form, and truncating we obtain

$$\tau_{max} = \frac{A}{r^{1/2}} + B \qquad (3)$$

where $A = K_I/(8\pi)^{1/2}$, and B is a constant containing σ^o_{nn}, σ^o_{zz}, σ^o_{nz}. Thus, the equation (3) can be rewritten as

$$\frac{\tau_{max}(8\pi r)^{1/2}}{\bar{\sigma}(\pi a)^{1/2}} = \frac{K_I}{\bar{\sigma}(\pi a)^{1/2}} + \frac{B(8\pi r)^{1/2}}{\bar{\sigma}(\pi a)^{1/2}} \qquad (4)$$

or

$$\frac{K_{ap}}{\bar{\sigma}(\pi a)^{1/2}} = \frac{K_I}{\bar{\sigma}(\pi a)^{1/2}} + \frac{B(8)^{1/2}}{\bar{\sigma}}(r/a)^{1/2} \qquad (5)$$

where $K_{ap} = \tau_{max}(8\pi r)^{1/2}$ is defined as the "apparent" stress intensity factor. If equation (5) is plotted as $K_{ap}/\bar{\sigma}(\pi a)^{1/2}$ vs $(r/a)^{1/2}$ where the value of τ_{max} is computed from the stress optic law, a sraight line extrapolated to the origin will give $K_I/\bar{\sigma}(\pi a)^{1/2}$, the normalized stress intensity factor.

Although this approach is good only for a uniform remote stress field with no surface present other than crack surfaces, if the linear zone can

---

* Stress optic law $\tau_{max} = Nf/2T$, where N, f and T are fringe number, material constant and slice thickness, respectively.

be determined by experimental data, the approach will still be valid. But if the linear zone cannot be located, other approaches must be used. Fortunately, no problems have yet been encountered which cannot be solved by using the method just described.

THE EXPERIMENTS

Models

The material which was used for this experiment was PSM-8F which is distributed by Photolastic Inc. Malvern, Pa.. This Transparent material has its own property. It is viscoelastic at room temperature, but becomes linearly elastic when heated above its critical temperature. Once the material is loaded above the critical temperature and cooled under load to room temperature, the fringes and deformations will be frozen into model. The steps for specimen preparation are as follows:

1) Drill and ream the hole to get a stress free hole surface in the center of the plate which is 7" wide by 23" long and drill holes at the ends of the plate to facilitate attachment to the loading fixture.
2) Tap a natural crack with a sharp blade at the edge of the hole perpendicular to the applied load.
3) Mount the test plate in a bending rig (Fig. 3) in the stress freezing oven and heat above the critical temperature. Then bend the plate to grow the crack to the desired length on the plate surface. Finally, under a small load, cool to room temperature by means of a programmed cam. Meanwhile, a bending calibration test (Fig. 4) is conducted to obtain the material fringe constant for each experiment. Next, the test specimen is mounted in a vertical position in the oven, heated above the critical temperature, and loaded in tension (Fig. 5) to grow the crack to the desired length in the hole surface. Then by reducing

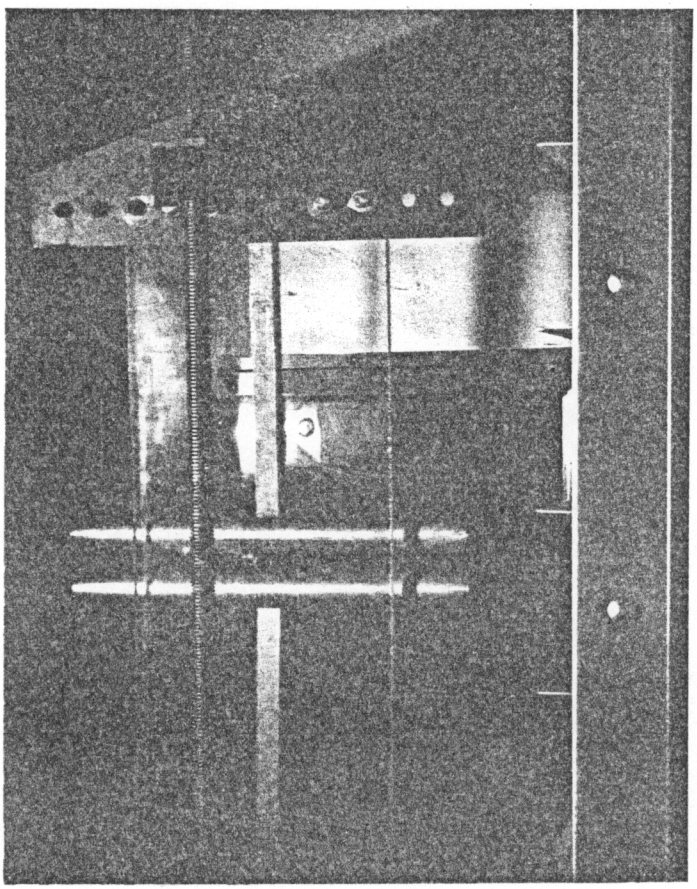

Fig. 3 Bending Setup

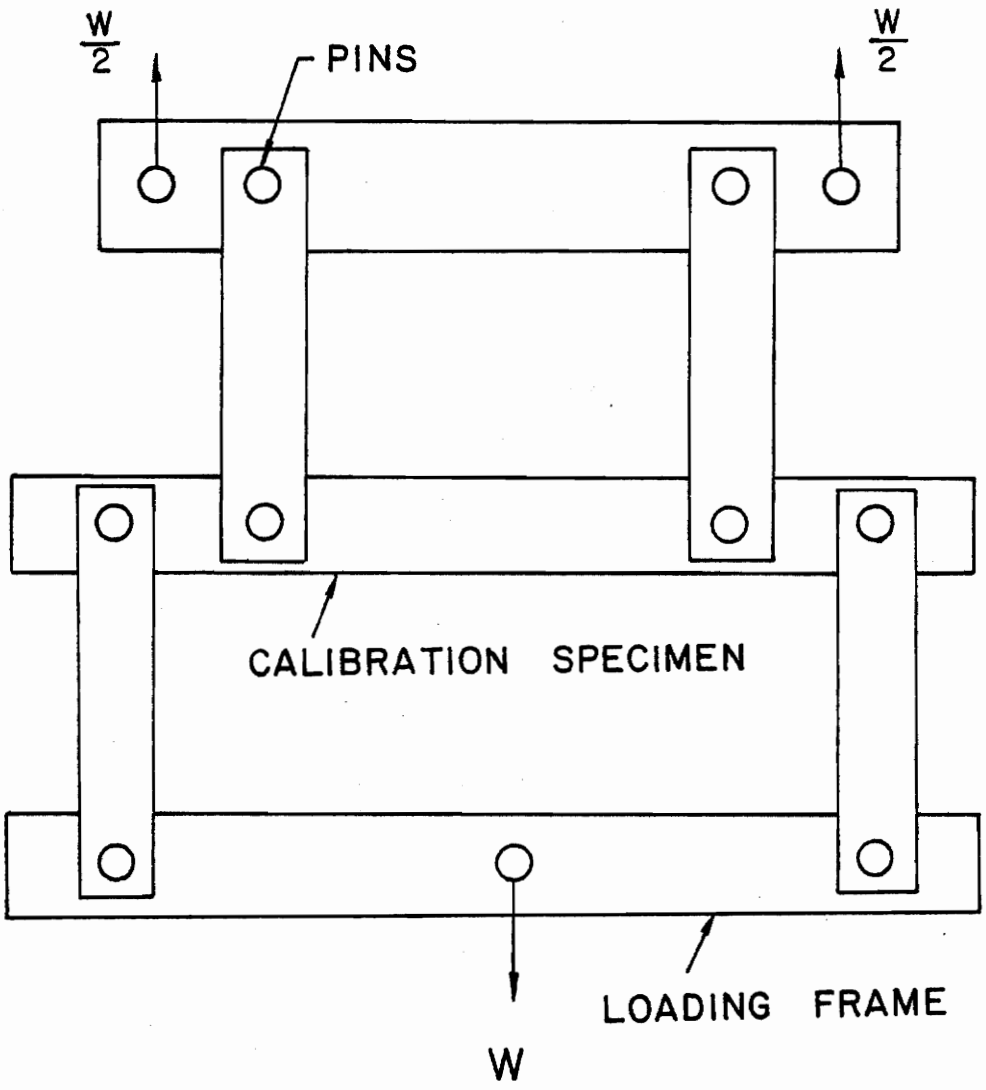

Fig. 4 Bending Calibration Test Setup

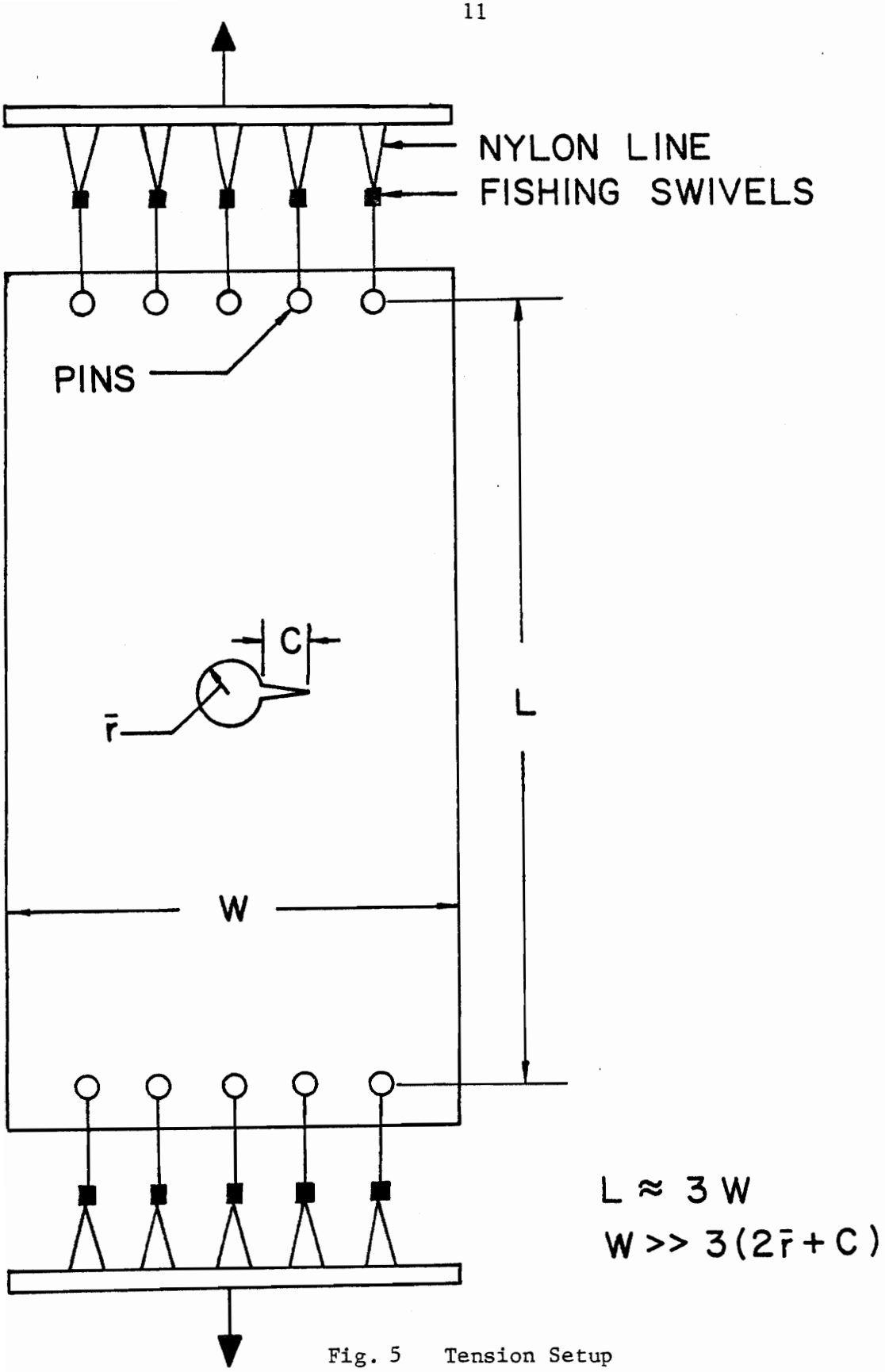

Fig. 5 Tension Setup

the load to one-third of the load which started to grow the crack to complete the rest of stress freezing cycle.

Test Procedure

When the oven cycle is completed, thin slices about 1.4 mm thick which are normal to both the crack front and the crack surface are cut from the specimen in the region H, S, and I (Fig 6). The slicing process is done with care so as to avoid adding machining stresses which would alter the already frozen in fringe pattern (22). Then slices are sanded smooth and coated with oil of the same index of refraction as the slice material and viewed under a crossed circular polariscope at 10x. By using the Tardy compensation method, the fractional fringe numbers are obtained versus their distance from the crack tip. Using this information, plus additional data including slice thickness, material fringe constant, and crack length, values of the normalized apparent stress intensity factor and normalized distance from the crack tip are obtained from a computer program which is available in the laboratory and then plotted. A representative plot may be seen on Figure 7. The darkened circles represent the data points which are considered to be within the linear zone. But those open points stand for the nonlinear zone which is resulted from the developing of material nonlinearities near the crack tip.

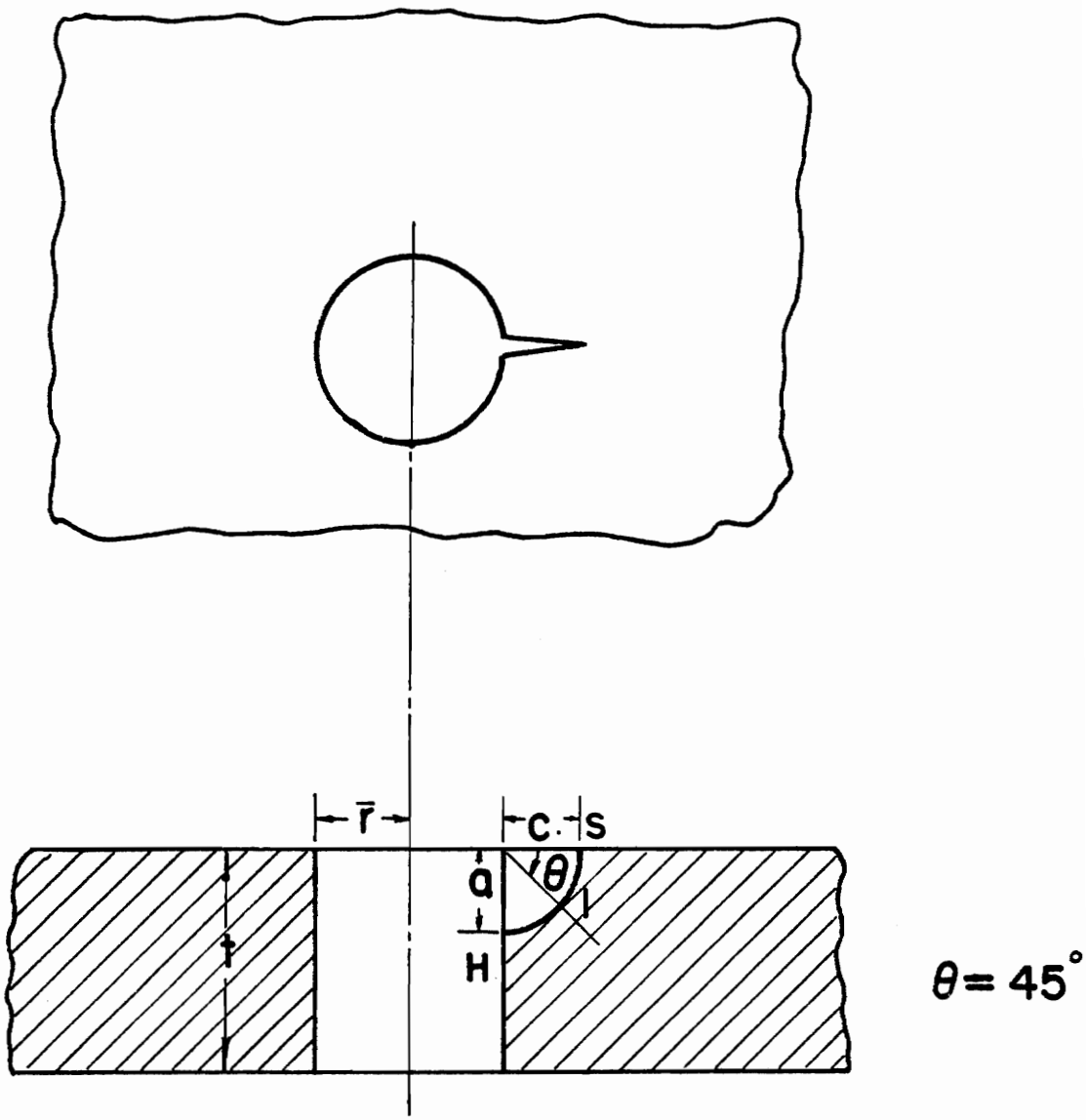

Fig. 6 Problem Geometry and Slice Locations

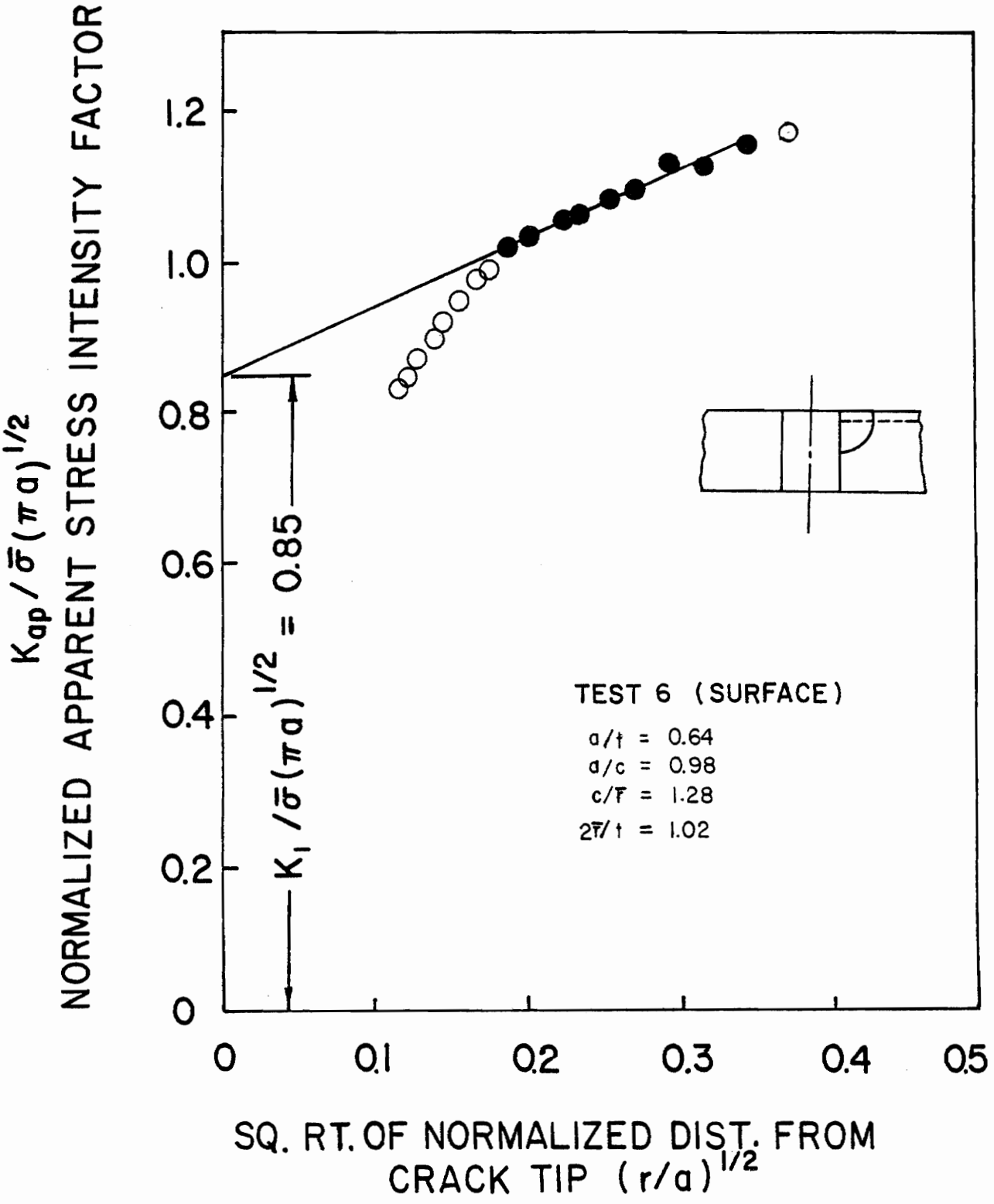

Fig. 7 Typical Data Set

RESULTS & DISCUSSION

The results of the seven tests are tabulated in Table V together with the predictions of the theories of Snow (23), Smith and Kullgren (24), Newman (25), Shah (26), Liu (27) and Hall and Finger (28). In each of the approaches by Newman, Liu, and Hall and Finger, there is a single value predicted for the SIF. In Newman's approach the SIF's were within 5% of the experimental values for the shallow flaw case, but disagreed in the neighborhood of 20% for deeper cracks. There was around 10% difference for both the shallow and moderate flaw cases in Liu's and Hall and Finger's theories, but the difference tended to increase for deeper flaws. The agreement with Snow's fatigue test was within 5% for the shallow flaw case, but there were no available solutions for moderate and deep crack cases. Only one of the seven tests has crack geometries close to those of existing finite element-alternating method results (24). For this theory there was about 6% difference on the hole surface and 15% difference on the plate surface.

The crack shapes from test 1 through 7 are presented in Figure 8. The crack shapes are quarter circular for $a/t < 0.3$, but exhibit a flattened region near the center of the flaw which invalidates the assumption of a circular crack shape when cracks go deeper. The same phenomenon is observed in nozzle cracks in reactor vessels (29, 30, 31). It is noted that crack shapes grown under monotonic loading by the photoelastic technique under a stable condition compares well with that of fatigue loading in steel under small strain yielding conditions (29).

The results of experiments and that of the finite element shown in test g of Table II might mislead one to believe that there existed very good agreement for deep cracks which exhibited a flattened region in the center of flaw border in the present study. But the results of test 5 and Figure 9 suggest that more than two points should be compared.

Although tests 4 and 5 exhibit very similar values of a/t, reference to Table III shows that values of a/c are 0.81 and 1.00 respectively and this is believed to be the major cause of the differences in SIF values exhibited in Figure 9.

For deeper cracks, the SIF distribution (Fig. 9) exhibits a maximum value near the center of the flaw border. However, there is a flattening near the center of the flaw border which indicates that the flaw growth will be less in the center than at other points along the border. It is conjectured that the effect of triaxial constraint which induces traction forces acting in the plane of the flaw surface causes an elevation of the SIF.

The frozen stress photoelastic results for a plate with a through natural crack at the edge are 12% higher than two dimensional solution (13). This is due to the variation of constraint caused by the change from a state of generalized plane strain near the crack tip to generalized plane stress remote from the crack tip. Since a transition zone must exist between these extremes, the problem becomes three dimensional and depends on Poisson's ratio. In photoelastic stress freezing experiments, ν=0.5 and in order to convert the results that would correspond to ν=0.3,

the photoelastic results are multiplied by a conversion factor

$$f = \frac{(1-(0.5))^{1/2}}{(1-(0.3))^{1/2}} = 0.91$$

If the conversion factor is applied to the edge crack problem, the difference between converted photoelastic stress freezing data and the two dimensional solution will be 3% which is within the engineering accuracy. The Poisson's ratio effect on surface flaws is less than 4% as shown by Smith (32). Based on these studies, the author believes the Poisson's ratio effect on the present experiment is within experimental error of 5%.

CONCLUSIONS & SUMMARY

1. A flattened region near the center of the crack is shown in tests 4, 5, 6, 7. This may be conjectured to have the tendency to reduce the gradient of stress intensity factor along the flaw border.
2. Self-similar crack growth can be produced for a penny shaped flaw in an infinite body where the SIF is constant along the flaw border. But non-self similar growth is developed in the hole-crack problem due to the complexity of the combination of hole, surface and back surface effects.
3. The variation in the SIF along the flaw border for deeper flaws is opposite that for shallow flaws (Fig. 9). This is believed to be related to an interaction between load redistribution and transverse constraint effects.
4. The least crack growth region (Fig. 8) corresponds to the maximum SIF (Fig. 9) which invalidates the assumption of constant material constants, C and m, in the crack growth rate equation.* In other words, C and m are geometry dependent.
5. The crack growth rate in the fatigue approach is the same as that of monotonic loading system, i.e. cracks grow more in the hole surface than on the plate surface as seen from tension-tension fatigue tests of Snow (25).
6. The major advantage of the stress freezing method is the ability to get the SIF's at the region of greatest interest. But one drawback of it is

---

*$da/dN = C\ (\Delta K)^m$

that it is impossible to find the SIF's from point to point continuously along the flaw border due to the finite thickness of the slice and also to the fact that the SIF determined from the slice is the average value across the slice thickness. Thus, the slice thickness should be kept as thin as possible with a sufficient number of fringe loops. According to previous experience, the error of the results is wuthin engineering accuracy, 5%, for slice thickness around 1 mm ~1.7 mm.

7. Since natural crack shapes for the deeper flaws differ from the simple shapes assumed in numerical solutions to this class of problems, and since the SIF is expected to be strongly influenced by the local geometry, it is suggested that use of the experimentally determined real crack shapes be incorporated into numerical solutions in order to lead to more accurate analytical predictions of SIF distribution.

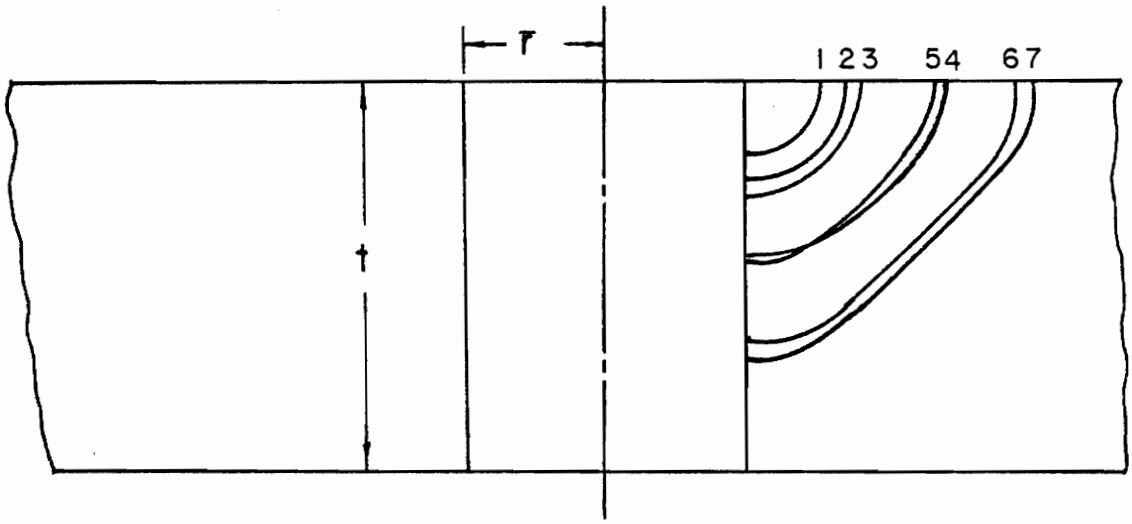

Fig. 8 Crack Shapes

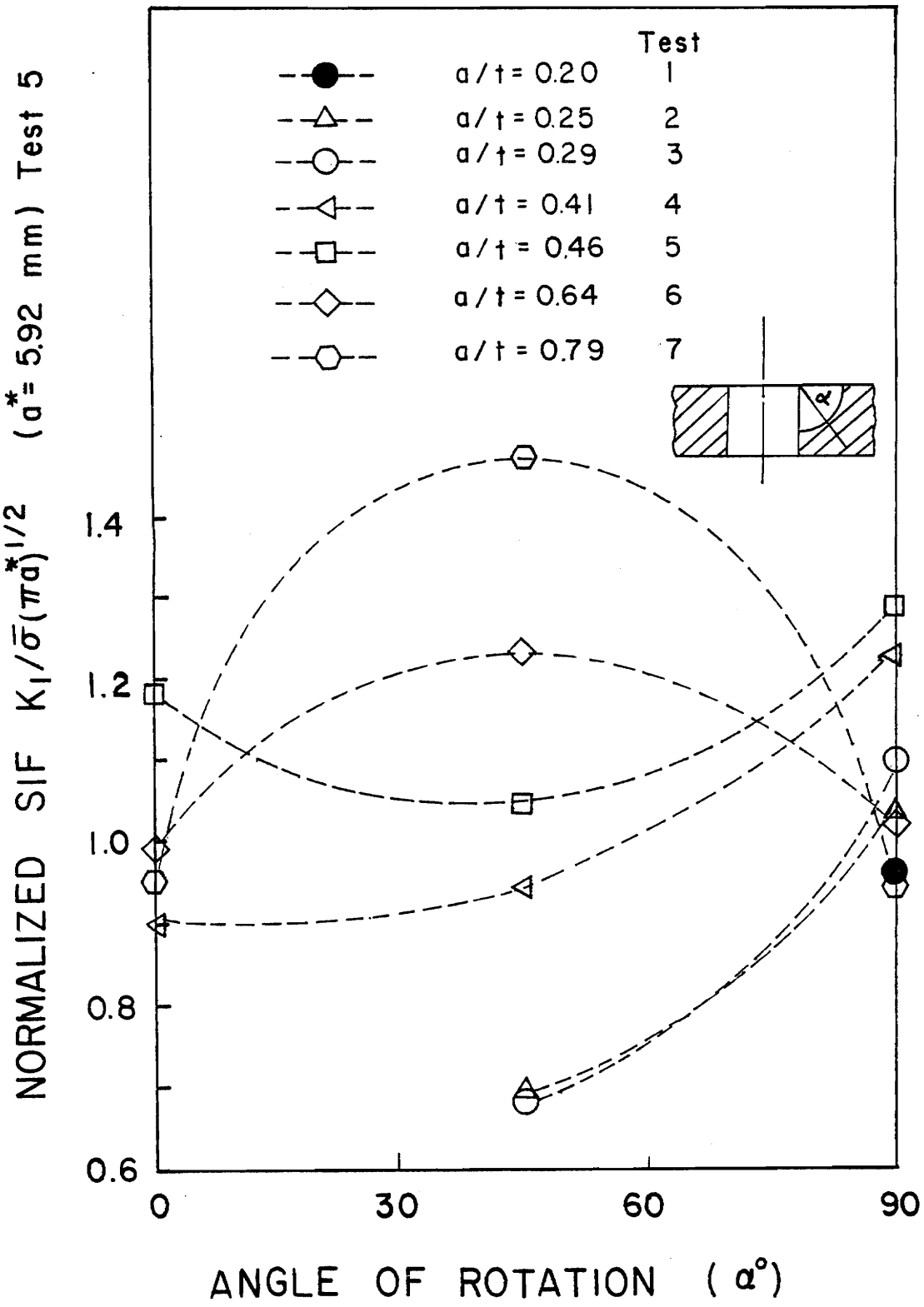

Fig. 9 Variation of SIF along the Crack Front

Appendix - Other Pertinent Theories, A Summary

1. Snow (23)

One of the experimental methods for solving three dimensional problems in fracture mechanics is to use the fatigue crack growth equation

$$da/dN = C\ (\Delta K)^m \qquad (6)$$

where da/dN = the crack growth rate

C, m = material constants, independent of geometry

ΔK = range of the SIF's applied to the specimen

In order to obtain a measurable crack growth rate, the applied K must be greater than K_{TH}, the threshold value of K, and less than K_{Ic}, fracture toughness. Snow's procedure to find the SIF's is as follows:

a. Determine the values of C and m from a single through-crack baseline test where da/dN was measured and ΔK was known.
b. Substitute values for C and m into equation (6) and measure the crack growth rate for the corner-crack at the edge of the hole, which will enable one to determine the SIF's by equation (6).

2. Smith and Kullgren (24)

The finite element technique must be considered as a powerful method to deal with complicated three dimensional problems. These investigators used the alternating method which consisted of two elastic solutions coupled by an iteration procedure to solve for the SIF's. The first solution is the

stress in an unflawed finite body due to the applied remote tensile force. Solution 1 produces a normal stress distribution, P, on the plane where the crack is to be located. The solution 2 is the stress in a finite body due to pressure, -P, applied to the surface crack. The iteration is continued until the stress on the crack surface of the finite body and the stress on the surface of the finite body are small. The superposition of the results gives the solution for the remote uniaxial loading on the finite body with crack where the crack surface is stress free and the finite body surface have the prescribed boundary conditions. The SIF's of Mode I will be found by adding the normal stress on the crack surface from all iterations.

The finite element mesh which is semicircular with 112 elements is shown in Figure 10 to model solution 1 of the finite element-alternating method for the crack configuration. There are seven divisions across the plate half-width and four layers of elements through the thickness. Planes inclined at 10°, 20° and 90° from the Z=0 plane further divide the plane. Finer divisions occupy the region of the hole where the crack is to be located to provide there a better definition of stress gradients.

Kullgren pointed out that the results in Ganong's paper (31) for the crack shapes of a/c=0.99 and 1.01 are subject to excessive errors, due to the large round-off errors of computer when the major and minor axes of the elliptical crack are nearly equal.

3. Newman (25)

Previous solutions for evaluating SIF's for a corner crack at the edge

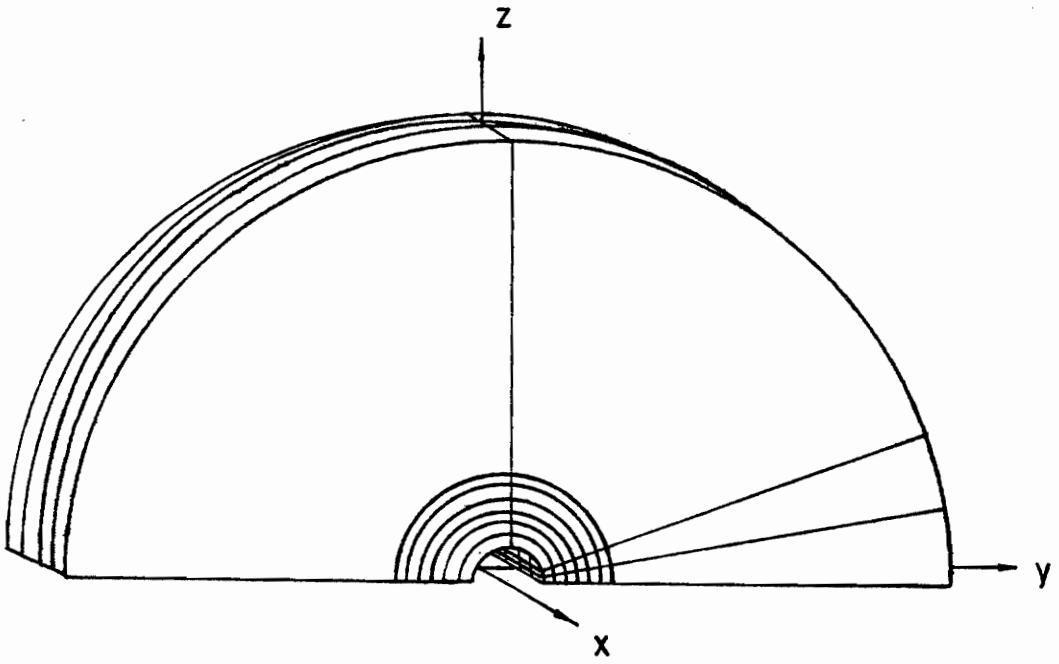

Fig. 10 112-Element Finite Element Mesh

of the hole were either restricted to limited regions or presented in graphical forms. Newman found empirical equations, reducing the complexity and computation. The only drawback in handling this type of problem is that it does not account for variation of SIF's along the crack front.

Newman applied the two parameter fracture criteria (TPFC) which relates the elastic stress intensity factor at failure, the nominal failure stress, and two material fracture parameters to the crack emanating from a circular hole in a finite plate subjected to the remote uniform stress. The stress intensity factor is expressed by

$$K_I = S(\pi a/Q)^{1/2} M_e f_1 (\sec \frac{\pi \bar{r}}{w})^{1/2}$$

$$M_1 = 1.2 - 0.1 \frac{a}{c} \qquad (0.02 \leq \frac{a}{c} \leq 1.0)$$

$$M_1 = (c/a)^{1/2}(1 + 0.1 \frac{a}{c}) \qquad (\frac{a}{c} > 1.0)$$

$$Q = 1 + 1.47(\frac{a}{c})^{1.64} \qquad (\frac{a}{c} \leq 1.0)$$

$$Q = 1 + 1.47(\frac{c}{a})^{1.64} \qquad (\frac{a}{c} > 1.0)$$

$$M_e = (M_1 + ((Qc/a)^{1/2} - M_1)(a/t)^p) f_w$$

$$p = 2 + 8(a/c)^3$$

$$f_w = (\sec(\frac{\pi}{2}(2\bar{r} + c)/(w - c)(a/t)^{1/2}))^{1/2}$$

$$f_1 = 0.707 - 0.18\lambda + 6.55\lambda^2 - 10.54\lambda^3 + 6.85\lambda^4$$

$$\lambda = \frac{1}{1 + \frac{c}{\bar{r}}}$$

Q = elastic shape factor

M_1 = front surface correction factor

M_e = back-face, front-face and finite width correction factor

f_w = finite width correction factor

f_1 = the Bowie correction for a through crack emanating from a circular hole

$(\sec \frac{\pi \bar{r}}{w})^{1/2}$ = a factor for an interaction between the hole and the finite width

w = plate width

4. Shah (26)

The expression (7) was determined by Shah (34) to solve the SIF's for open quarter-elliptical single crack at the corner of the hole

$$K_{I1p} = M_F(a/c, \beta)\, M_B(a/c, a/t, \beta)\, (\frac{2\bar{r}+\pi ac/4t}{2\bar{r}+2\pi ac/4t})^{1/2}\, K_{Ih} \qquad (7)$$

where K_{Ih} is the SIF's for two-semi elliptical embedded cracks at the hole. By introducing the stress free front surface correction, $M_F(a/c, \beta)$, Shah found the SIF's for double elliptical cracks in a semi-infinite solid. This correction factor was assumed to be independent of θ for $0 < \theta < 90$,

and was expressed by

$$M_F(a/c, \beta) = 1.0 + 0.12(1 - a/2c)^2$$

In order to estimate the SIF's for one quarter elliptical corner crack at the edge of the hole, he introduced both a back surface correction factor, $M_B(a/c, a/t, \beta)$, which can be found in the reference, and a conversion factor from double corner cracks to single corner crack, $\left(\frac{2\bar{r}+\pi ac/4t}{2\bar{r}+2\pi ac/4t}\right)^{1/2}$. It was pointed out that the fracture will initiate at a point about 25° away from the hole surface where the crack tip deformation builds up to a level equivalent to a plane strain condition.

5. Liu (27)

An approximate expression was derived for a corner flaw emanating from an edge of a quarter infinite solid by using the Smith (35) solution for a semi-circular flaw. The stress intensity factor for a quarter circular flaw was obtained, superimposing with the Kobayashi (36) back correction factor and the Bowie (37) circular hole influence factor

$$K_I = 1.12\bar{\sigma}(2a)^{1/2}\alpha_b F(L/\bar{r})$$

with $L=a/\sqrt{2}$ and where α_b and $F(L/\bar{r})$ factors were presented in his paper.

6. Hall and Finger (28)

Hall and Finger generated starter cracks by electrical discharge machining and subjected the specimen to fatigue loading to grow the crack

to the final dimension. It was assumed the failure initiated along the peripheries of the flaws under conditions of plane strain at the region of the hole surface. They proposed the fracture criteria:

$$K_I = C\bar{\sigma}\sqrt{a}\ F(c/2\bar{r})\ G(a/t)\ H(\bar{r}/t)$$

where C=1.1, $H(r/t)=(4\bar{r}/t)^{1/2}$ and $F(c/2\bar{r})$ and $G(a/t)$ were presented graphically from test data. Their approach is only valid for the case $a/c < 1$.

TABLE I

TEST GEOMETRIES FOR THE PREVIOUS EXPERIMENT

Test Number	a	b	c	d	e	f	g	h
Hole Radius ($\bar{r}$) mm	6.35	6.35	4.83	6.35	4.83	6.35	6.35	4.83
Plate Depth (t) mm	14.7	23.6	19.3	14.5	19.8	13.7	13.5	19.8
Crack Length (c) mm	2.79	3.56	9.65	6.35	7.62	4.06	5.08	7.37
Crack Depth (a) mm	2.54	5.59	8.38	6.86	9.65	6.35	9.91	15.2
Remote Stress($\bar{\sigma}$) kPa	99	108	85	75	81	88	71	62
a/t	0.18	0.24	0.43	0.48	0.49	0.46	0.74	0.78
a/c	0.95	1.59	0.86	1.10	1.27	1.55	1.98	2.05
$c/\bar{r}$	0.43	0.56	2.02	0.98	1.60	0.63	0.79	1.56
$2\bar{r}/t$	0.87	0.54	0.49	0.88	0.48	0.94	0.95	0.48

TABLE II

COMPARISONS WITH OTHER ANALYTICAL THEORIES IN THE PREVIOUS EXPERIMENT

Test Number	a	b	c	d	e	f	g	h
STRESS INTENSITY FACTORS			(Experimental Results)					
Surface $K_s/\bar{\sigma}(\pi a)^{1/2}$	1.17	0.99	0.71	0.90	0.86	0.98	0.95	0.72
Hole $K_h/\bar{\sigma}(\pi a)^{1/2}$	1.91	1.34	1.12	0.89	0.98	1.24	1.08	0.72
$(K_s + K_h)/2\bar{\sigma}(\pi a)^{1/2}$	1.54	1.17	0.92	0.90	0.92	1.11	1.02	0.72
			(Analytical Results)					
Newman $K_I/\bar{\sigma}(\pi a)^{1/2}$	1.25	1.07	0.80	0.94	0.77	1.04	0.90	0.70
Smith $K_s/\bar{\sigma}(\pi a)^{1/2}$	--	--	--	1.03	--	1.04	0.95	--
Smith $K_h/\bar{\sigma}(\pi a)^{1/2}$	--	--	--	1.36	--	1.24	1.06	--
Snow $K_s/\bar{\sigma}(\pi a)^{1/2}$	--	1.15	--	--	1.08	1.06	--	--
Snow $K_h/\bar{\sigma}(\pi a)^{1/2}$	--	1.40	--	--	1.16	1.28	--	--
Shah $K_s/\bar{\sigma}(\pi a)^{1/2}$	1.31	1.16	0.77	0.97	0.84	1.10	0.96	0.76
Shah $K_h/\bar{\sigma}(\pi a)^{1/2}$	1.75	1.22	1.36	1.38	1.15	1.22	1.00	0.86

TABLE III

TEST GEOMETRIES FOR THE PRESENT EXPERIMENT

Test Number		1	2	3	4	5	6	7
Hole Radius ($\bar{r}$)	mm	6.35	6.35	6.35	6.35	6.35	6.35	6.35
Plate Depth (t)	mm	12.8	12.9	13.1	12.6	12.9	12.4	13.9
Crack Length (c)	mm	2.36	3.30	3.81	6.35	5.89	8.13	11.3
Crack Depth (a)	mm	2.54	3.30	3.81	5.16	5.92	8.00	11.1
Remote Stress($\bar{\sigma}$)	kPa	49.7	70.3	43.8	76.5	70.5	61.7	55.4
a/t		0.20	0.25	0.29	0.41	0.46	0.64	0.79
a/c		1.07	1.00	1.00	0.81	1.00	0.98	0.98
$c/\bar{r}$		0.37	0.52	0.60	1.00	0.93	1.28	1.78
$2\bar{r}/t$		0.99	0.98	0.97	1.01	0.99	1.02	0.91

TABLE IV

COMPARISONS WITH OTHER ANALYTICAL THEORIES IN THE PRESENT EXPERIMENT

Test Number		1	2	3	4	5	6	7
STRESS INTENSITY FACTORS			(Experimental Results)					
Surface	$K_s/\bar{\sigma}(\pi a)^{1/2}$	--	--	--	0.95	1.19	0.85	0.69
Hole	$K_h/\bar{\sigma}(\pi a)^{1/2}$	1.47	1.39	1.37	1.32	1.29	0.89	0.69
Intermediate	$K_m/\bar{\sigma}(\pi a)^{1/2}$	--	0.94	0.85	1.01	1.05	1.06	1.08
	$(K_s+K_h+K_m)/3\bar{\sigma}(\pi a)^{1/2}$	1.47	1.17	1.11	1.08	1.18	0.93	0.82
STRESS INTENSITY FACTORS (% Difference)			(Analytical Results)					
Snow	$K_h/\bar{\sigma}(\pi a)^{1/2}$	1.53 (4%)	1.46 (5%)	1.44 (5%)	--	--	--	--
Smith*	$K_s/\bar{\sigma}(\pi a)^{1/2}$	--	--	--	--	1.03 (15%)	--	--
Smith*	$K_h/\bar{\sigma}(\pi a)^{1/2}$	--	--	--	--	1.36 (6%)	--	--
Newman	$K_I/\bar{\sigma}(\pi a)^{1/2}$	1.46 (1%)	1.12 (4%)	1.08 (3%)	0.98 (10%)	0.92 (24%)	0.83 (10%)	0.74 (9%)
Hall	$K_I/\bar{\sigma}(\pi a)^{1/2}$	--	1.30 (10%)	1.21 (8%)	1.19 (11%)	1.08 (9%)	1.05 (12%)	0.95 (14%)
Liu	$K_I/\bar{\sigma}(\pi a)^{1/2}$	--	1.32 (11%)	1.29 (15%)	--	1.11 (6%)	1.04 (11%)	0.94 (13%)
Shah	$K_s/\bar{\sigma}(\pi a)^{1/2}$	--	--	--	0.86 (4%)	0.92 (14%)	0.83 (1%)	0.73 (5%)
Shah	$K_h/\bar{\sigma}(\pi a)^{1/2}$	1.75 (19%)	1.60 (13%)	1.62 (15%)	1.55 (15%)	1.48 (20%)	1.39 (36%)	1.29 (46%)
Shah	$K_m/\bar{\sigma}(\pi a)^{1/2}$	--	1.20 (21%)	1.18 (30%)	1.48 (22%)	1.00 (5%)	0.90 (15%)	0.81 (25%)

* The geometry for this SIF is $a/c=1.1$, $a/t=0.5$, $2\bar{r}/t=1.0$.

REFERENCES

1. Jolles, M., McGowan, J. J., and Smith, C. W., "Stress Intensity for Cracks Emanating from Holes in Finite Thickness Plates", VPI-E-75-15, August 1975.

2. Gran, R. J., Oranzio, F. D., Paris, P. L., Irwin, G. R. and Hertzberg, R. "Investigation and Analysis Development of Early Life Aircraft Structure Failures", AFFDL-TR-70-1439, 1971.

3. Post, D., "Photoelastic Stress Analysis for an Edge Crack in a Tensile Field", Proceedings,Society for Experimental Stress Analysis, Vol. 16, No. 1, 1954, pp. 99-116.

4. Well, A. A. and Post, D., "The Dynamic Stress Distribution Surrounding a Running Crack - A Photoelastic Analysis", Proceedings, Society for Experimental Stress Analysis, Vol. 16, No. 1, 1958, pp. 69-92.

5. Marloff, R. H., Leven, M. M., Johnson, R. L. and Ringler, T. M., "Photoelastic Determination of SIF's", Experimental Mechanics, Vol. 11, No. 12, December 1971, pp. 529-539.

6. Fessler, J. and Mansell, D. O., " Photoelastic Study of Stresses Near Cracks in Thick Plates", Journal of Mechanical Engineering Science, Vol. 4, No. 3, 1962, pp. 213-225.

7. Bradley, W. B. and Kobayashi, A. S., "A Investigation of Propagating Cracks by Dynamic Photoelasticity", Journal of Experimental Mechanics, Vol. 10, No. 3, March 1970, pp. 106-113.

8. Bradley, W. B. and Kobayashi, A. S., "Fracture Dynamics - A Photoelastic Investigation", Journal of Engineering Fracture Mechanics. Vol. 3, No. 3, October 1971, pp. 317-322.

9. Kobayashi, A. S., Wade, B. G., Bradley, W. B. and Chiu, S. T., " Crack Branding in Homalite - 100 Sheets", TR-13, Department of Mechanical Engineering, College of Engineering, University of Washington, Seattle, Washington. June 1972.

10. Kobayashi, A. S. and Wade, B. G., "Crack Propagating and Arrest in Impected Plates", TR-14, Department of Mechanical Engineering, College of Engineering, University of Washington, Seattle, Washington. July 1972.

11. Smith, D. G. and Smith, C. W., "A Photoelastic Investigation of Closure and Other Effects upon Local Bending Stresses in Cracked Plates",

International Journal of Fracture Mechanics, Vol. 6, No. 3, September 1970, pp. 305-318.

12. Smith, D. G. and Smith, C. W., "Photoelastic Determination of Mixed Mode Stress Intensity Factors", Engineering Fracture Mechanics, Vol. 4, No. 3, 1972, pp. 357-366.

13. Smith, C. W., McGowan, J. J. and Jolles, M., "Effects of Artificial Cracks and Poisson's Ratio upon Photoelastic Stress Intensity Determination", Experimental Mechanics, Vol. 16, No. 5, May 1976, pp. 188-193.

14. McGowan, J. J. and Smith, C. W., "Stress Intensity Factors for Deep Cracks Emanating from the Corner Formed by a Hole Intersecting a Plate Surface", Mechanics of Crack Growth, ASTM STP 590, American Society for Testing and Materials, 1976, pp. 460-476.

15. Jolles, M., McGowan, J. J. and Smith, C. W., "Use of a Hybrid Computer Assisted Photoelastic Technique for Stress Intensity Determination in Three-Dimensional Problems", Computational Fracture Mechanics, ASME-AMD-SP Proceedings of Second National Congress on Pressure Vessels and Piping, E. F. Rybicki and S. E. Benzley, eds., 1975, pp. 63-82.

16. Smith, C. W., Jolles, M., and Peters, W. H., "Stress Intensity Determination in Three-Dimensional Problems by the Photoelastic Method", Proceedings of the Second International Conference on Mechanical Behavior of Materials, 1976, pp. 235-239.

17. Smith, C. W., Jolles, M. and Peters, W. H., "Stress Intensities for Cracks Emanating from Pin Loaded Holes", (In Press) Progress in Flaw Growth and Fracture, ASTM-STP 631, 1977.

18. Smith, C. W., Jolles, M. and Peters, W. H., "Stress Intensities in Flawed Pressure Vessels", Proceedings of the Third International Conference on Pressure Vessel Technology, Part II Materials and Fabricatien, Tokyo, ASME, April 1977, pp. 535-544.

19. Forman, R. G., Kearney, V. E. and Engle, R. M., "Numerical Analysis of Crack Propagation in Cyclic-Loaded Structures", Transaction of ASME, Journal of Basic Engineering, Vol. 89, No. 3, 1967.

20. Irwin, G. R., "Discussion", Proceedings of the Society for Experimental Stress Analysis, Vol. 16, No. 1, 1958, pp. 92-96.

21. Kassir, M. and Sih, G. C., "Three Dimensional Stress Distribution Around an Elliptical Crack Under Arbitrary Loadings", Journal of Applied Mechanics, Vol. 33, No. 3, pp. 601-611, 1966.

22. Hetenyi, M., "The Fundamentals of Three-Dimensional Photoelasticity", Journal of Applied Mechanics. Transaction ASME, Vol. 5, No. 4, 1958, pp. 149-155.

23. Snow, J. R., "A SIF Calibration for Corner Flaws at an Open Hole", AFML-TR-74-282, 1975.

24. Smith. F. W. and Kullgren, T. E., "Theoretical and Experimental Analysis of Surface Cracks Emanating from Fastner Holes", AFFPL-TR-76-104, 1976.

25. Newman, J. C., "Predicting Failures of Specimens with Either Surface Cracks or Corner Cracks at Holes", NASA-TN-D-8244, June 1976.

26. Shah, R. C., "SIFs for Through and Part-Through Cracks Originating at Fastner Holes", Presented at the Eighth National Symposium on Fracture Mechanics, Brown University, Providence, R. Z., August 1974.

27. Liu, A. F., "SIF for a Corner Flaw", Engineering Fracture Mechanics, Vol. 4, 1972, pp. 175-179.

28. Hall, L. R. and Finger, R. W., "Fracture and Fatigue Growth of Partially Embedded Flaws", Proceedings of the Air Force Conference on Fatigue and Fracture of Aircraft Structures and Material, AFFDL-TR-70-144, U. S. Air Force Systems Command, Wright-Patterson AFB, Ohio, September 1970, pp. 235-262.

29. Broekhoven, M. J. G., "Fatigue and Fracture Behavior of Cracks at Nozzle Corners; Comparison of Theoretical Predictions with experimental Data", Proceedings of the Third International Conference of Pressure Vessel Technology - Part II Materials and Fabrication, Tokyo, April 1977, (ASME) pp. 839-852.

30. Sommer, E., "Experimental Methods for the Determination of Stress Intensity Factors under Various Loading Conditions", Prospects of Fracture Mechanics, Noordhoff - International Publishing Co., June 1974, pp. 593-607.

31. Smith, C. W., Peters, W. H. and Jolles, M. I., "Stress Intensity Factors for Reactor Vessel Nozzle Cracks", Presented at the Energy Technology Conference and Exhibit, Houston, Texas, September 18-22, 1977.

32. Smith, F. W. "Stress Intensity Factors for a Surface Flawed Fracture Specimen". TR-1, Department of Mechanical Engineering, Colorado State University.

33. Ganong, G. P., "Quarter-Elliptical Cracks Emanating from Holes in

Plates", Ph. D Thesis, Department of Mechanical Engineering, Colorado State University, July 1975.

34. Shah, R. C. and Kobayashi, A. S., "SIF's for the Elliptical Crack Approaching the Surface of a Semi-Infinite Solid", International Journal of Fracture Mechanics, Vol. 9, 1973, pp. 133-146.

35. Smith, F. W., Emery, A. F. and Kobayashi, A. S., "SIF's for Semi-Circular Cracks, Part II, Semi-Infinite Solid", Vol. 34, Transaction ASME. Vol. 89, 1967, pp. 953-959.

36. Kobayashi, A. S. and Moss, W. L., "Surface Intensity Magnification Factors for Surface-Flawed Tension Plates and Notched Round Tension Bar", Proceedings of the Second International Conference on Fracture, Brighton, England, 1968.

37. Bowie, O. L., "Analysis of an Infinite Plate Containing Radial Cracks Originating at the Bonding of an Internal Circular Hole", Journal of Mathematics and Physics, Vol. 35, 1956, pp. 60-71.

VITA

The author was born in Taipei, Taiwan on May 28, 1950. After having finished his middle school, he entered Tatung Institute of Technology in the summer of 1966, five years later he received an ASME degree. Two years military service in the National Chinese Army and two years working experience in Yue-Loong motor company as a maintenance engineer followed his academic career. In 1974 he decided to pursue higher education in United States. Then in the summer of 1976 he enrolled in the Tuskegee Institute as a 4^{th} year student. One year later he got his BS degree in the ME department and also received an assistantship from the Engineering Science & Mechanics department of Virginia Polytechnic Institute & State University.

Shaufa Gou

DETERMINATION OF STRESS INTENSITY FACTORS FOR CRACKS EMANATING FROM HOLES IN FINITE THICKNESS PLATES

by

Shau-Fen Gou

(ABSTRACT)

The stress freezing photoelastic method is a proven technique for the estimation of stress intensity factors along crack fronts in complex three dimensional problems. Comparisons between previous photoelastic and approximate analytical results have revealed discrepancies in results for the case where the crack shape is nearly quarter circular. In the present study, the frozen stress photoelastic method was applied to such geometries with varying flaw depth. Results are compared with those of other investigators. It is concluded that the flaw growth in this problem is non-self similar due to the complexity of boundary shapes. The variation of the stress intensity factor along the crack front is also studied.